

Measurement of Dipolar Couplings for Methylene and Methyl Sites in Weakly Oriented Macromolecules and Their Use in Structure Determination

Marcel Ottiger,* Frank Delaglio,* John L. Marquardt,* Nico Tjandra,† and Ad Bax*

*Laboratory of Chemical Physics, National Institute of Diabetes and Digestive and Kidney Diseases, †Laboratory of Biophysical Chemistry, National Heart, Lung, and Blood Institute, National Institutes of Health, Bethesda, Maryland 20892-0520

Received May 20, 1998

A simple and effective method is described for simultaneously measuring dipolar couplings for methine, methylene, and methyl groups in weakly oriented macromolecules. The method is a *J*-modulated 3D version of the well-known [¹H-¹³C] CT-HSQC experiment, from which the *J* and dipolar information are most accurately extracted by using time-domain fitting in the third, constant-time dimension. For CH₂-sites, the method generally yields only the sum of the two individual ¹³C-¹H couplings. Structure calculations are carried out by minimizing the deviation between the measured sum, and the sum predicted for each methylene on the basis of the structure. For rapidly spinning methyl groups the dipolar contribution to the splitting of the outer ¹³C quartet components can be used directly to constrain the orientation of the C-CH₃ bond. Measured sidechain dipolar couplings are in good agreement with an ensemble of NMR structures calculated without use of these couplings. © 1998 Academic Press

Key Words: dipolar couplings; molecular alignment; liquid crystal; protein; structure determination; sidechain dynamics; ubiquitin.

If a small degree of macromolecular alignment with the magnetic field is induced either by the molecule's own magnetic susceptibility anisotropy (1–6) or by using a very dilute liquid crystalline phase (7–9), dipolar couplings no longer average to zero. If the alignment is sufficiently weak, the high-resolution character of the NMR spectrum is maintained and the largest (mainly one-bond) dipolar couplings between pairs of atoms manifest themselves as changes in the corresponding *J* splittings (4–9). For ¹H-¹³C couplings in proteins, measurements so far have been restricted to the ¹³C^α-¹H^α pairs. These can be measured directly from a 2D ¹H-¹³C correlation spectrum, recorded in the absence of heteronuclear decoupling in either the ¹H or ¹³C dimension (8) or, in cases where overlap in such a *J*-coupled 2D spectrum is too severe, from a 3D triple resonance (HA)CA-(CO)NH experiment without ¹H decoupling during ¹³C^α evolution (10). Another procedure measures the ¹J_{CH} splitting from the intensity modulation in a series of constant-time (CT) ¹³C-¹H HSQC spectra, where a *J*-dephasing time is included in the CT evolution period (11). Here, we demonstrate that this latter ap-

proach is easily adapted to enable measurement of CH₂ and CH₃ couplings and yields highly reproducible results. Although for methylene sites only the sum of the two ¹J_{CH} splittings can be determined reliably in this manner, the change in this sum value between the isotropic and aligned states can be used directly in structure calculations and has a restraining power comparable to that of a single ¹³C-¹H dipolar coupling.

The pulse scheme of the *J*-modulated CT-HSQC experiment is shown in Fig. 1. For methine sites, the observed signal, after Fourier transformation in the *t*₁ and *t*₃ dimensions, is simply given by

$$S(F_1, t_2, F_3) = A \cos[\pi(^1J_{CH})t_2] \prod_k \cos[\pi(J_{CHk} + D_{CHk})t_2] \quad [1]$$

where *A* is the intensity of the corresponding resonance in the first 2D spectrum (at *t*₂ = 0), and *J*_{CHk} and *D*_{CHk} refer to the multi-bond scalar and dipolar interaction between the ¹³C and proton *k*. Note that although *J* couplings to protons more than 3 bonds away from the ¹³C are usually vanishingly small, this does not necessarily apply to the dipolar coupling. However, as *J*_{CHk} + *D*_{CHk} is typically much smaller than (4*T*)⁻¹, where 2*T* is the duration of the ¹³C constant-time evolution period (2*T* = 1/*J*_{CC} ≈ 28 ms), such multi-bond interactions remain unresolved if a Fourier transformation is carried out in the *t*₂ dimension and merely result in an apparent decay of the signal in the *t*₂ dimension. This decay is well approximated by the Gaussian function, $\exp(-at_2^2)$, with *a* = $\sum_k \pi^2 (J_{CHk} + D_{CHk})^2 / 2$.

For CH₂ sites, the magnetization immediately after the first INEPT transfer is described by $2S_y I_z^1 + 2S_y I_z^2$, where *I*¹ and *I*² are the spin operators for the two protons. *J*-dephasing as a result of the one-bond interactions yields

$$\begin{aligned} S_y I_z^1 \rightarrow & S_y I_z^1 \cos(\pi J_1 t_2) \cos(\pi J_2 t_2) \\ & - 2S_x I_z^1 I_z^2 \cos(\pi J_1 t_2) \sin(\pi J_2 t_2) \\ & - S_y I_z^2 \sin(\pi J_1 t_2) \sin(\pi J_2 t_2), \end{aligned} \quad [2]$$

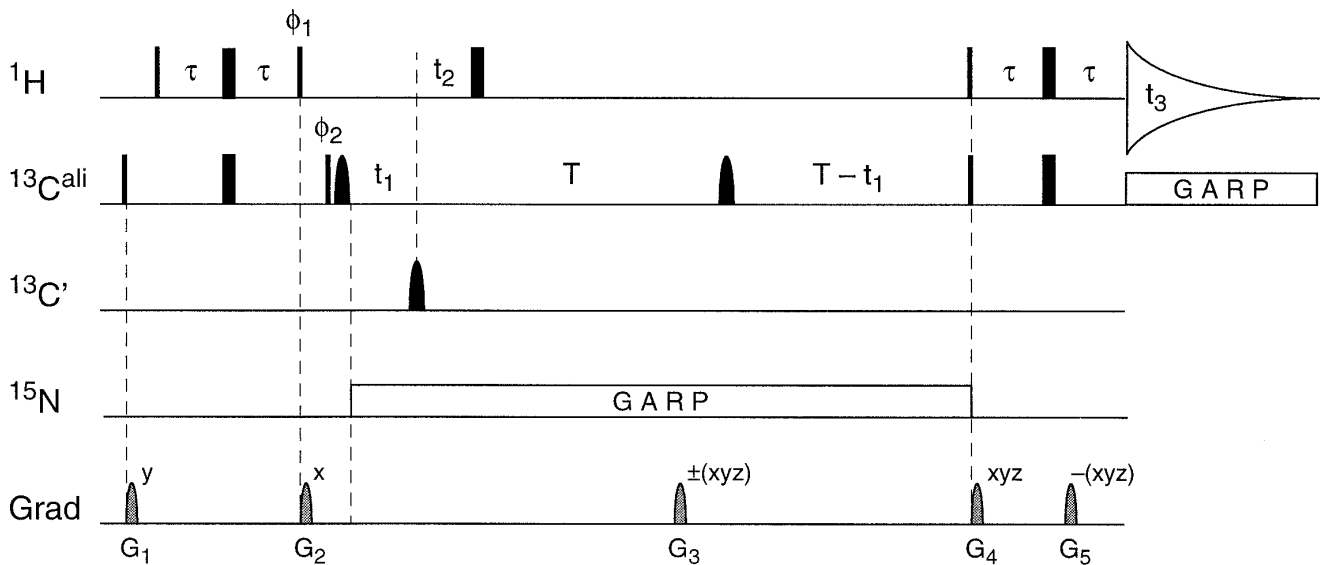


FIG. 1. Pulse scheme of the J -modulated [^{13}C - ^1H] CT-HSQC experiment. Narrow and wide pulses correspond to 90° and 180° flip angles, respectively, with phase x , unless indicated. The shaped $^{13}\text{C}^{\text{ali}}$ pulses (carrier at 43 ppm) are of the hyperbolic secant type, with a squareness level of 3, and a duration of $500 \mu\text{s}$ (20). The first shaped $^{13}\text{C}^{\text{ali}}$ serves to eliminate offset-dependent phase errors caused by the 180° refocusing pulse. The $^{13}\text{C}'$ 180° pulse is sine-bell shaped and has a duration of $4/\Delta\delta$ (where $\Delta\delta$ is the difference in resonance frequency in Hertz between the ^{13}C carrier and the center of the carbonyl region). All other pulses are applied at high power. Delay durations, $\tau = 1.5 \text{ ms}$; $2T = 28 \text{ ms}$. Phase cycling, $\phi_1 = y, -y; \phi_2 = x, x, y, y, -x, -x, -y, -y$ for negative G_3 gradient; $\phi_2 = x, x, -y, -y, -x, -x, y, y$ for positive G_3 gradient; Rec. = $x, -x, y, -y, -x, x, -y, y$. All gradients are sine-bell shaped with 25 G/cm at their center. Gradient durations, $G_{1,2,3,4,5} = 4, 3.5, 3.95, 0.7, 0.3 \text{ ms}$. Quadrature in the t_1 dimension is obtained by coherence transfer pathway selection. The duration of gradient G_3 was carefully tuned in order to maximize magnetization transfer from ^{13}C to ^1H . For each t_1 duration, two FIDs are acquired, one with a negative polarity of G_3 , and one with a positive polarity. The sum and difference of this pair of FIDs provide the two components of the t_1 quadrature signal (21).

where $J_n = ^1J_{\text{CH}_n} + ^1D_{\text{CH}_n}$. Only the first and last terms on the right-hand side of [2] are transferred back into magnetization observable during t_3 . Assuming that these transfers occur with equal efficiency, and using $\cos(\pi J_1 t_2) \cos(\pi J_2 t_2) - \sin(\pi J_1 t_2) \sin(\pi J_2 t_2) = \cos[\pi(J_1 + J_2)t_2]$ then yields an observed signal, $S(F_1, t_2, F_3)$, modulated by $J_1 + J_2$:

$$S(F_1, t_2, F_3) = A \cos[\pi(^1J_{\text{CH}1} + ^1D_{\text{CH}1} + ^1J_{\text{CH}2} + ^1D_{\text{CH}2})t_2] \times \prod_k \cos[\pi(J_{\text{CH}k} + D_{\text{CH}k})t_2]. \quad [3a]$$

Thus, only the outer lines of the methylene triplet are observed if a Fourier transformation with respect to t_2 is carried out, and only the sum of the coupling between the ^{13}C and its two attached protons can be obtained from this data.

For rapidly spinning methyl groups, the couplings between ^{13}C and its three attached protons are indistinguishable from one another, and $S(F_1, t_2, F_3)$ is given by

$$S(F_1, t_2, F_3) = A \{3 \cos[3\pi(^1J_{\text{CH}} + ^1D_{\text{CH}})t_2] + \cos[\pi(^1J_{\text{CH}} + ^1D_{\text{CH}})t_2]\} \times \prod_k \cos[\pi(J_{\text{CH}k} + D_{\text{CH}k})t_2]. \quad [3b]$$

After t_2 Fourier transformation, the outer quartet components are three times more intense than the inner components and as the frequency of these outer components is three times more sensitive to changes in $^1J_{\text{CH}} + ^1D_{\text{CH}}$ than the inner components, the dipolar contributions are derived most accurately from the components modulated by $3\pi(^1J_{\text{CH}} + ^1D_{\text{CH}})$.

Fourier transformation does not provide the best means for extracting the frequency of a signal that is highly truncated in the time domain. Apodization of the t_2 time domain data, normally used to avoid serious truncation wiggles in the FT spectrum, most attenuates the data points taken at the largest t_2 values, i.e., the points which are most sensitive to the small changes in $^1J_{\text{CH}} + ^1D_{\text{CH}}$ of interest. Because the t_2 modulation pattern consists of only one or two cosine functions of known phase, decaying in an approximately Gaussian manner, a more accurate way to obtain the frequencies is to fit the non-apodized time domain data directly using a least-squares procedure. The highest t_2 modulation frequencies occur for methyl groups: $\frac{3}{2}(^1J_{\text{CH}} + ^1D_{\text{CH}})$. For the small degrees of alignment typically used in liquid crystal protein NMR, these values are invariably smaller than 250 Hz, and a t_2 dwell time as large as 2 ms is adequate to avoid aliasing in this dimension. Considering that the total CT duration is only 28 ms ($\sim 1/J_{\text{CC}}$), a minimum of only 15 t_2 increments is needed. Note that no

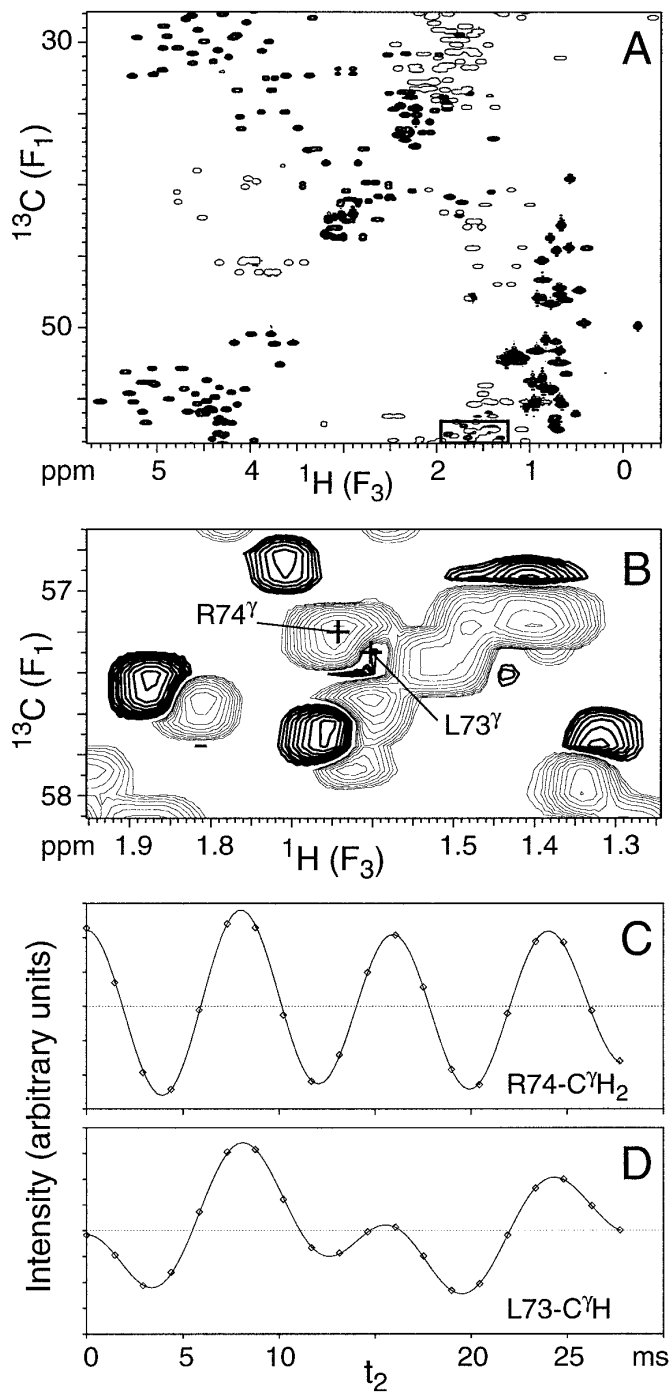


FIG. 2. Cross sections through the $S(F_1, t_2, F_3)$ data matrix obtained with the scheme of Fig. 1 for uniformly $^{13}\text{C}/^{15}\text{N}$ -enriched ubiquitin (0.7 mM) in a liquid crystalline phase consisting of 5% (w/v) phospholipids (in a 3:1 molar ratio of DMPC and DHPC) in 93% $\text{H}_2\text{O}/7\%$ D_2O , pH 6.5, 10 mM phosphate buffer, 37°C. (A) The first plane ($t_2 = 0$), corresponding to the regular CT-HSQC spectrum. Extensive aliasing in the F_1 dimension is used, and positive and negative peaks are drawn as thin and thick contours. Note the excellent level of water suppression. (B) Expanded region of the boxed area in (A). (C) t_2 interferogram, taken at the F_1, F_3 coordinates of Arg $^{74}\text{-C}^\gamma\text{H}_2$. Time-domain fitting yields a main component with a modulation frequency of 113.2 Hz and a slightly weaker component (corresponding to Arg $^{74}\text{-C}^\gamma\text{H}_2$) modulated at 250.2 Hz. All couplings were extracted using an automated scheme within the NMRPipe processing package (22), with J -modulation curves (t_2 -interferograms) taken at positions obtained from peak-picking the Fourier-transformed spectrum. Interpolation in the F_1/F_3 dimensions is obtained by extracting a small part of the $S(F_1, t_2, F_3)$ matrix, centered around the F_1/F_3 coordinate of interest, followed by inverse FT in F_1 and F_3 , extensive zero-filling, and forward FT in F_1 and F_3 . Frequencies were obtained from the t_2 interferograms by least-squares optimized fitting to a sum of Gaussian-damped cosine functions, where the number of frequency components and their initial frequencies were determined by finding signals in the Fourier transform of the interferogram.

quadrature detection is used in t_2 . When using least-squares fitting in the t_2 dimension, an even smaller number of increments could be used, but either a systematic search or some other procedure such as the maximum entropy method (12) would be required for obtaining the initial frequency estimates.

The J -modulated CT-HSQC experiment is demonstrated for a 0.7 mM sample of uniformly $^{13}\text{C}/^{15}\text{N}$ enriched ubiquitin (VLI research, Southwestern, PA) in a 220- μl Shigemi microcell (Allison Park, PA), containing 5% w/v bicelles (3:1 DMPC:DHPC) in 93% $\text{H}_2\text{O}/7\%$ D_2O , pH 6.5. Figure 2A shows the aliphatic region of the spectrum acquired for $t_2 = 0$. The excellent resolution obtained in [^1H - ^{13}C] CT-HSQC spectra results in well resolved resonances for the vast majority of resonances. An expanded view of the most crowded region is shown in Fig. 2B. Spectral overlaps which occur in the 2D spectrum between a methyl and methylene, or between a methylene and a methine resonance, can be resolved by the distinctly different t_2 modulation patterns and both sets of couplings can be determined reliably. This is illustrated in Figs. 1C and 1D, which show the t_2 interferograms for the overlapping resonances of Arg $^{74}\text{-C}^\gamma\text{H}_2$ and Leu $^{73}\text{-C}^\gamma\text{H}$. The drawn lines represent the calculated best-fit least-squares function, consisting of the sum of two Gaussian-damped cosine functions. The accuracy of the measurement can be assessed by comparing the two splittings measured for pairs of non-equivalent methylene protons. For methylenes with non-degenerate ^1H frequencies, the t_2 modulation frequencies have a root-mean-square pairwise difference of less than 0.4 Hz, which is much better than the precision needed to measure the generally much larger dipolar contributions. Analogously, the separation of the weak inner two lines of methyl quartets differs by a root-mean-square deviation of less than 0.3 Hz from one-third of the splitting measured more accurately for the intense outer quartet components.

By taking the difference in modulation frequency at 25°C, where the solution is isotropic, and at 36°C, where the sample is liquid crystalline, accurate dipolar contributions could be measured for 91 (out of 97) aliphatic methine sites, for 100 (out of 111) methylenes, and for 48 (out of 50) methyl groups.

250.1 Hz and a 8-fold weaker component (corresponding to the edge of the partly overlapping signal of Leu $^{73}\text{-C}^\gamma\text{H}$) modulated at 111.1 Hz. (D) t_2 interferogram, taken at the F_1, F_3 coordinates of Leu $^{73}\text{-C}^\gamma\text{H}$. Time-domain fitting yields a main component with a modulation frequency of 113.2 Hz and a slightly weaker component (corresponding to Arg $^{74}\text{-C}^\gamma\text{H}_2$) modulated at 250.2 Hz. All couplings were extracted using an automated scheme within the NMRPipe processing package (22), with J -modulation curves (t_2 -interferograms) taken at positions obtained from peak-picking the Fourier-transformed spectrum. Interpolation in the F_1/F_3 dimensions is obtained by extracting a small part of the $S(F_1, t_2, F_3)$ matrix, centered around the F_1/F_3 coordinate of interest, followed by inverse FT in F_1 and F_3 , extensive zero-filling, and forward FT in F_1 and F_3 . Frequencies were obtained from the t_2 interferograms by least-squares optimized fitting to a sum of Gaussian-damped cosine functions, where the number of frequency components and their initial frequencies were determined by finding signals in the Fourier transform of the interferogram.

Structure calculation. The procedure used to incorporate the dipolar couplings into the XPLOR-based (14) protein structure calculation has been described previously (15, 16). In brief, a tetra-atomic pseudomolecule OXYZ is defined where the OX, OY, and OZ bond vectors are orthogonal to one another. The O atom of this molecule is defined at a fixed position in space, away from the protein. An energy penalty function term E_{dip} is defined which accounts for the difference between an observed dipolar coupling, and the one predicted if the orientation of the alignment tensor were to correspond to that of OXYZ. As OXYZ freely reorients, it aligns itself to yield a best fit to the observed couplings during the simulated annealing process.

For methines, E_{dip} is given by

$$E_{\text{dip}} = k(D_{\text{CH}}^{\text{calc}} - D_{\text{CH}}^{\text{obs}})^2. \quad [4a]$$

For methylenes, where only the sum of D_{CH_1} and D_{CH_2} is measured, E_{dip} is simply given by

$$E_{\text{dip}} = k(D_{\text{CH}_1}^{\text{calc}} + D_{\text{CH}_2}^{\text{calc}} - D_{\text{CH}_1}^{\text{obs}} - D_{\text{CH}_2}^{\text{obs}})^2. \quad [4b]$$

For tetrahedral methyl groups, rapid rotation scales the $^{13}\text{C}-^1\text{H}$ dipolar coupling by $-\frac{1}{3}$. Thus, the threefold larger change in splitting observed for the outer methyl quartet components is exactly opposite to that predicted for a proton located on the C-CH₃ bond vector, at the regular distance removed from the methyl carbon. As all constants related to bond length and gyromagnetic ratios are absorbed in the constants used in the XPLOR routine, no separate pseudoatom needs to be defined and the dipolar contribution to the outer quartet splitting, after multiplication by -1 , can be used directly to constrain the orientation of the C-CH₃ bond.

Effect of internal dynamics. Rapid fluctuations of bond vector orientations relative to the alignment tensor of the macromolecule reduce the magnitude of the dipolar coupling relative to a static bond vector along the time-averaged orientation. This scaling parameter corresponds to the generalized order parameter S , which usually has a large and relatively uniform value in the 0.85–0.95 range for most backbone atoms. However, for sidechains the variation in internal dynamics is much more pronounced (17), and the measured dipolar splitting only provides a lower limit for the dipolar coupling expected for the time-averaged orientation of such a site. Unless quantitative information on sidechain rigidity is available, we propose it is safest to define the penalty function as a half-open square well,

$$\begin{aligned} E_{\text{dip}} &= k(D_{\text{CH}}^{\text{calc}} - D_{\text{CH}}^{\text{obs}})^2 && \text{for } |D_{\text{CH}}^{\text{obs}}| > |D_{\text{CH}}^{\text{calc}}| \\ E_{\text{dip}} &= 0 && \text{for } |D_{\text{CH}}^{\text{obs}}| \leq |D_{\text{CH}}^{\text{calc}}|. \end{aligned} \quad [5]$$

This is fully analogous to the way in which NOEs are commonly converted only into upper, but not into lower bound distance restraints (18).

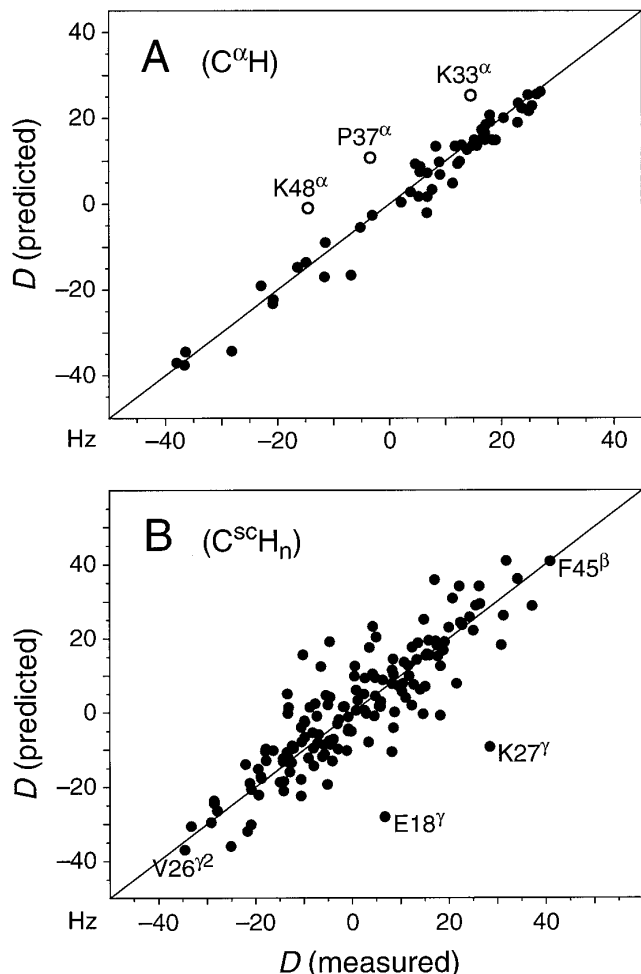


FIG. 3. Plots of one-bond $^{13}\text{C}-^1\text{H}$ dipolar couplings in human ubiquitin calculated on the basis of its structure versus measured couplings, (A) for the backbone $^{13}\text{C}^{\alpha}-\text{H}^{\alpha}$ using the crystal structure, and (B) for the aliphatic sidechains using a set of 30 NMR structures calculated without use of sidechain C-H dipolar couplings. The alignment tensor was calculated from a best fit to the dipolar couplings for the $^{13}\text{C}^{\alpha}-\text{H}^{\alpha}$ pairs of residues 1–71; residues 33, 37, and 48 were not used because there is further NMR evidence that the conformation of these residues differs in the crystal and solution structures. For methylenes, the sum of the two $^1\text{H}-^{13}\text{C}$ dipolar couplings is presented. For methyl groups, the measured dipolar coupling is multiplied by -3 (i.e., the change in splitting measured for the outer quartet components multiplied by -1), so as to correspond to a $^{13}\text{C}-^1\text{H}$ coupling in the C-CH₃ direction (see text).

The sum of $^1D_{\text{CH}_1} + ^1D_{\text{CH}_2}$ values for tetrahedral methylene groups spans the same range as that of individual $^1D_{\text{CH}}$ couplings. For a uniform distribution of methylene group orientations, the sum of the two methylene dipolar couplings (where both protons have the same spin state) results in a fully asymmetric dipolar coupling powder pattern ($\eta = 1$), with its most populated position at zero. When using the square-well definition of Eq. [5], summed dipolar couplings measured for methylenes are therefore slightly less effective at restraining

the structure than an individual $^1D_{\text{CH}}$ value. The latter yields an axially symmetric powder pattern and has a smaller fraction of orientations that yield near-zero couplings. Experiments for measuring individual $^1D_{\text{CH}}$ values for methylene sites are presently being explored.

Figure 3A compares the $^{13}\text{C}^\alpha$ - $^1\text{H}^\alpha$ dipolar couplings measured in ubiquitin with those predicted by its 1.8-Å crystal structure (19), using an orientation and magnitude of the alignment tensor which minimizes the root-mean-square between measured and predicted couplings. Residues 33, 37, and 48 were excluded in this fit as other dipolar couplings for these residues also give poor agreement with the crystal structure. Using the same alignment tensor, Fig. 3B compares the dipolar couplings measured in ubiquitin with the average dipolar couplings calculated for an ensemble of 30 solution structures, derived without the use of sidechain dipolar couplings. The correlation coefficient for these data (including the two outliers, Lys 27 -C $^\gamma$ H₂ and Glu 18 -C $^\gamma$ -H₂) is 0.85. This is considerably better than for the lowest energy NMR structure alone ($R = 0.75$), or the crystal structure ($R = 0.66$) (data not shown), and confirms that the ensemble of NMR structures provides a better representation than any individual structure. However, it is also noteworthy that, on average, the magnitudes of the dipolar couplings measured for the sidechains are only marginally (~10%) smaller than calculated for the static crystal structure. This suggests that for many of the sidechains conformational averaging is perhaps not as extensive as sometimes assumed. A more quantitative analysis of these sidechain dipolar couplings in terms of dynamics is currently underway in our laboratory.

ACKNOWLEDGMENTS

We thank Dennis Torchia and Marius Clore for useful discussions. This work was supported by the AIDS Targeted Anti-Viral Program of the Office of the Director of the National Institutes of Health.

REFERENCES

- C. Gayathri, A. A. Bothner-By, P. C. M. van Zijl, and C. MacLean, Dipolar magnetic field effects in NMR spectra of liquids, *Chem. Phys. Lett.* **87**, 192–196 (1982).
- E. W. Bastiaan, C. MacLean, P. C. M. Van Zijl, and A. A. Bothner-By, High resolution NMR of liquids and gases: Effects of magnetic-field-induced molecular alignment, *Ann. Rep. NMR Spectrosc.* **9**, 35–77 (1987).
- A. A. Bothner-By, Magnetic field induced alignment of molecules, in "Encyclopedia of Nuclear Magnetic Resonance" (D. M. Grant and R. K. Harris, Eds.), pp. 2932–2938, Wiley, Chichester (1996).
- J. R. Tolman, J. M. Flanagan, M. A. Kennedy, and J. H. Prestegard, Nuclear magnetic dipolar interactions in field-oriented proteins: information for structure determination in solution, *Proc. Natl. Acad. Sci. USA* **92**, 9279–9283 (1995).
- H. C. King, K. Y. Wang, I. Goljer, and P. H. Bolton, Magnetic alignment of duplex and quadruplex DNAs, *J. Magn. Reson. B* **109**, 323–325 (1995).
- N. Tjandra, S. Grzesiek, and A. Bax, Magnetic field dependence of nitrogen-proton J splittings in ^{15}N -enriched human ubiquitin resulting from relaxation interference and residual dipolar coupling, *J. Am. Chem. Soc.* **118**, 6264–6272 (1996).
- A. Bax and N. Tjandra, High resolution NMR of human ubiquitin in an aqueous liquid crystalline medium, *J. Biomol. NMR* **10**, 289–292 (1997).
- N. Tjandra and A. Bax, Direct measurement of distances and angles in biomolecules by NMR in a dilute liquid crystalline medium, *Science* **278**, 1111–1114 (1997).
- M. Ottiger and A. Bax, Characterization of magnetically oriented phospholipid micelles for measurement of dipolar couplings in macromolecules, *J. Biomol. NMR*, in press.
- N. Tjandra and A. Bax, Large variations in $^{13}\text{C}^\alpha$ chemical shift anisotropy in proteins correlate with secondary structure, *J. Am. Chem. Soc.* **119**, 9576–9577 (1997).
- N. Tjandra and A. Bax, Measurement of dipolar contributions to $^1J_{\text{CH}}$ splittings from magnetic field dependence of J modulation in two-dimensional NMR spectra, *J. Magn. Reson.* **124**, 512–515 (1997).
- P. Schmieder, A. S. Stern, G. Wagner, and J. C. Hoch, Improved resolution in triple resonance spectra by nonlinear sampling in the constant-time domain, *J. Biomol. NMR* **4**, 483–490 (1994).
- C. R. Sanders and J. P. Schwonek, Characterization of magnetically orientable bilayers in mixtures of DHPC and DMPC by solid-state NMR, *Biochemistry* **31**, 8898–8905 (1992).
- A. T. Brünger, "XPLOR Manual Version 3.1," Yale University, New Haven, CT (1993).
- N. Tjandra, D. S. Garrett, A. M. Gronenborn, A. Bax, and G. M. Clore, Defining long-range order in NMR structure determination from the dependence of heteronuclear relaxation times on rotational diffusion anisotropy, *Nature Struct. Biol.* **4**, 443–449 (1997).
- G. M. Clore, A. M. Gronenborn, and N. Tjandra, Direct structure refinement against residual dipolar couplings in the presence of rhombicity of unknown magnitude, *J. Magn. Reson.* **131**, 159–162 (1998).
- D. Yang, T. Mittermaier, Y.-K. Mok, and L. E. Kay, A study of protein sidechain dynamics from ^2H auto-correlation and ^{13}C cross correlation NMR spectroscopy: Application to the N-terminal SH3 domain from drk, *J. Mol. Biol.* **276**, 939–954 (1998).
- K. Wüthrich, "NMR of Proteins and Nucleic Acids," p. 177, Wiley, New York (1986).
- S. Vijay-Kumar, C. E. Bugg, and W. J. Cook, Structure of ubiquitin refined at 1.8 Å resolution, *J. Mol. Biol.* **194**, 531–544 (1987).
- M. S. Silver, R. I. Joseph, and D. I. Hoult, Highly selective $\pi/2$ and π pulse generation, *J. Magn. Reson.* **59**, 347–351 (1984).
- P. Bachmann, W. P. Aue, L. Müller, and R. R. Ernst, Phase separation in two-dimensional NMR spectroscopy, *J. Magn. Reson.* **28**, 29 (1977).
- F. Delaglio, S. Grzesiek, G. W. Vuister, G. Zhu, J. Pfeifer, and A. Bax, NMRPipe: A multidimensional spectral processing system based on UNIX pipes, *J. Biomol. NMR* **6**, 277–293 (1995).